Received: 21 February 2023 | Revised: 25 February 2024 | Accepted: 23 April 2024

DOI: 10.1002/ecy.4366

ARTICLE

ECOLOGY
ECOLOGICAL SOCIETY OF AMERICA

Remotely sensed crown nutrient concentrations modulate forest reproduction across the contiguous United States

Tong Qiu[1,2] | **James S. Clark**[2,3] | **Kyle R. Kovach**[4] | **Philip A. Townsend**[4] | **Jennifer J. Swenson**[5]

[1]Department of Ecosystem Science and Management, The Pennsylvania State University, University Park, Pennsylvania, USA

[2]Nicholas School of the Environment, Duke University, Durham, North Carolina, USA

[3]Universite Grenoble Alpes, Institut National de Recherche pour Agriculture, Alimentation et Environnement (INRAE), Laboratoire EcoSystemes et Societes En Montagne (LESSEM), St. Martin-d'Heres, France

[4]Department of Forest and Wildlife Ecology, University of Wisconsin Madison, Madison, Wisconsin, USA

[5]Center for Geospatial Analysis, The College of William and Mary, Williamsburg, Virginia, USA

Correspondence
Tong Qiu
Email: tvq5043@psu.edu

Funding information
National Science Foundation, Grant/Award Number: DEB-1754443; National Science Foundation Belmont Forum, Grant/Award Number: 1854976; National Aeronautics and Space Administration (NASA) Advanced Information Systems Technology, Grant/Award Numbers: 16-0052, 18-0063; National Aeronautics and Space Administration (NASA) Earth Science Applications: Ecological Conservation, Grant/Award Number: 80NSSC23K1534; Programme d'Investissement d'Avenir under project FORBIC, Grant/Award Number: 18-MPGA-0004; NSF Macrosystems Biology and NEON-Enabled Science, Grant/Award Number: DEB-1638720; NSF Biology Integration Institute, Grant/Award Number: DBI-2021898

Handling Editor: Anthony W. D'Amato

Abstract

Global forests are increasingly lost to climate change, disturbance, and human management. Evaluating forests' capacities to regenerate and colonize new habitats has to start with the seed production of individual trees and how it depends on nutrient access. Studies on the linkage between reproduction and foliar nutrients are limited to a few locations and few species, due to the large investment needed for field measurements on both variables. We synthesized tree fecundity estimates from the Masting Inference and Forecasting (MASTIF) network with foliar nutrient concentrations from hyperspectral remote sensing at the National Ecological Observatory Network (NEON) across the contiguous United States. We evaluated the relationships between seed production and foliar nutrients for 56,544 tree-years from 26 species at individual and community scales. We found a prevalent association between high foliar phosphorous (P) concentration and low individual seed production (ISP) across the continent. Within-species coefficients to nitrogen (N), potassium (K), calcium (Ca), and magnesium (Mg) are related to species differences in nutrient demand, with distinct biogeographic patterns. Community seed production (CSP) decreased four orders of magnitude from the lowest to the highest foliar P. This first continental-scale study sheds light on the relationship between seed production and foliar nutrients, highlighting the potential of using combined Light Detection And Ranging (LiDAR) and hyperspectral remote sensing to evaluate forest regeneration. The fact that both ISP and CSP decline in the presence of high foliar P levels has immediate application in improving

forest demographic and regeneration models by providing more realistic nutrient effects at multiple scales.

KEYWORDS
foliar nutrients, forest regeneration, hyperspectral remote sensing, leaf spectroscopy, LiDAR, NEON, seed production, tree fecundity, tree reproduction

INTRODUCTION

Understanding the regeneration potential of forests recovering from disturbance, climate change, and harvest (Curtis et al., 2018; Duane et al., 2021; McDowell et al., 2020) is a goal of global change research (Clark et al., 2021). Colonization capacity starts with the seed production of individual trees by species, size, and habitat conditions that vary across regions. Seed production is often simplified and represented as a constant fraction of net primary production (NPP) in the Dynamic Global Vegetation Models (DGVMs) (Fisher et al., 2018; Hanbury-Brown et al., 2022). This approximation, while useful for large-scale modeling, overlooks the variations in seed production driven by environmental factors and species-specific traits. A first synthesis of species-level differences in foliar nutrient and seed production at the global scale showed large differences among species (Qiu et al., 2022). The explanation for these species differences and how they might inform landscape regeneration requires knowledge of individual tree nutrient status across gradients of climate and fertility. Even in a large plant trait database like TRY (Kattge et al., 2020), less than 5% of species have individual trait data for nitrogen (N) and phosphorous (P). Information on important nutrients such as potassium (K), calcium (Ca), and magnesium (Mg) remains unavailable. Moreover, trait databases cannot provide insight in which nutrient effects must be combined with individual attributes, such as size, competition, and local fertility gradients—these individual-scale interactions require observations of all variables from the same trees. The data coverage required to span variation in seed production and order-of-magnitude variation between individual trees and within trees over time (Clark et al., 2004) has not been available. For these reasons, studies of within-species responses to fertility have been limited in biogeographic extent and species coverage (Bazzaz et al., 2000; Fernández-Martínez et al., 2017). Here we provided a first quantification of seed production and three primary (N, P, and K) and two secondary (Ca and Mg) foliar macronutrients by synthesizing hyperspectral imagery from the National Ecological Observatory Network (NEON) with fecundity data from the Masting Inference and Forecasting (MASTIF) network. We demonstrate a continental-scale role for foliar P, which is associated with low tree fecundity in a majority of species. Responses to other foliar nutrients depend on species differences in nutrient demand, with biogeographic gradients accounting for additional variation in seed production. At the community level, seed production decreased four orders of magnitude along the foliar P gradient, but with additional sensitivity to other nutrients.

The literature on tree fecundity and nutrients conflates processes that engage different scales of variation (Figure 1). If N–P–K treatment increases seed production in the current or following year, should we expect seed production to also increase along natural fertility

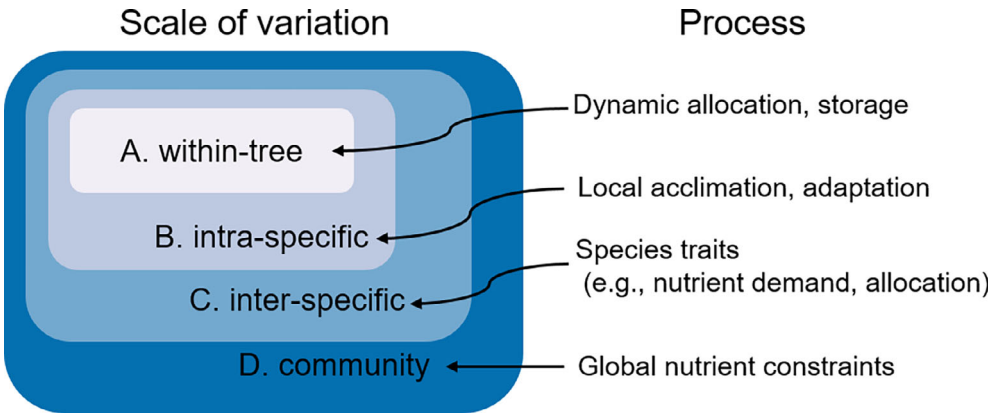

FIGURE 1 Four scales of variation in nutrient effects on fecundity and the processes they engage shown at the righthand side.

gradients? Should we expect that species found only on fertile sites will produce more seed than those restricted to infertile sites? The dynamic relationships between fecundity, tissue concentrations, and/or added nutrients for an individual (scale A) provide evidence on how storage and shifting allocation can contribute to masting cycles (Berdanier & Clark, 2016; Davis et al., 2004; Ran et al., 2008; Sala et al., 2012). Much of this evidence comes from nutrient addition experiments (Davis et al., 2004; Ran et al., 2008), but there are also several studies that track internal concentrations across years of varying seed production (Han et al., 2008; Sala et al., 2012). Variations between individuals, either along natural fertility gradients or receiving different nutrient treatments (scale B), provide insight into a species' response to fertility. Because allocation to fecundity can vary with site differences in nutrient supply or ratios, individuals of a species can show a positive or negative association with fertility gradients (Qiu et al., 2022). Differences between species in these responses to nutrients (scale C) can help to explain community composition. For example, temperate deciduous species (e.g., *Acer* and *Quercus*) tend to be more nutrient-demanding than conifers (e.g., *Abies*, *Pinus*, and *Picea*; Figure 2). Spatial variation in seed production by the community (scale D) provides insight into global relationships between seed production and fertility. Landscape variation in fecundity, or community seed productivity (CSP), combines individual variation (scale B) with species turnover (scale C). For example, there are 250-fold changes in fecundity from dry taiga to wet tropics (Journe et al., 2022). However, Qiu et al. (2022) did not find the effects of fertility indices on CSP, potentially because responses within species were neutralized by species turnover. The responses at these different scales engage different processes, from dynamic allocation (A) to acclimation and adaptation along natural gradients (B) to species differences (C). The spatial variation in CSP combines them (D).

There is scale dependence not only in processes, but also in data. Qiu et al. (2022) disentangled the effects of scales B, C, and D relative to fertility indices associated with global maps. However, individual nutrient conditions could diverge from the spatially coarse gridded products. The individual condition depends not only on broad-scale variation in parent material and drainage, that is, the scales available to global gridded products, but also on microtopography and the local competitive environment (Clark et al., 2014). The association between fecundity and nutrients at scales B through D remains unknown.

A convergence of airborne sensing tools, foliar measurements, and fecundity monitoring, allows us to evaluate the individual-scale interactions that shape continental-scale potential for regeneration. A comprehensive understanding of nutrient effects on fecundity requires methods that can be implemented remotely across broad areas, while

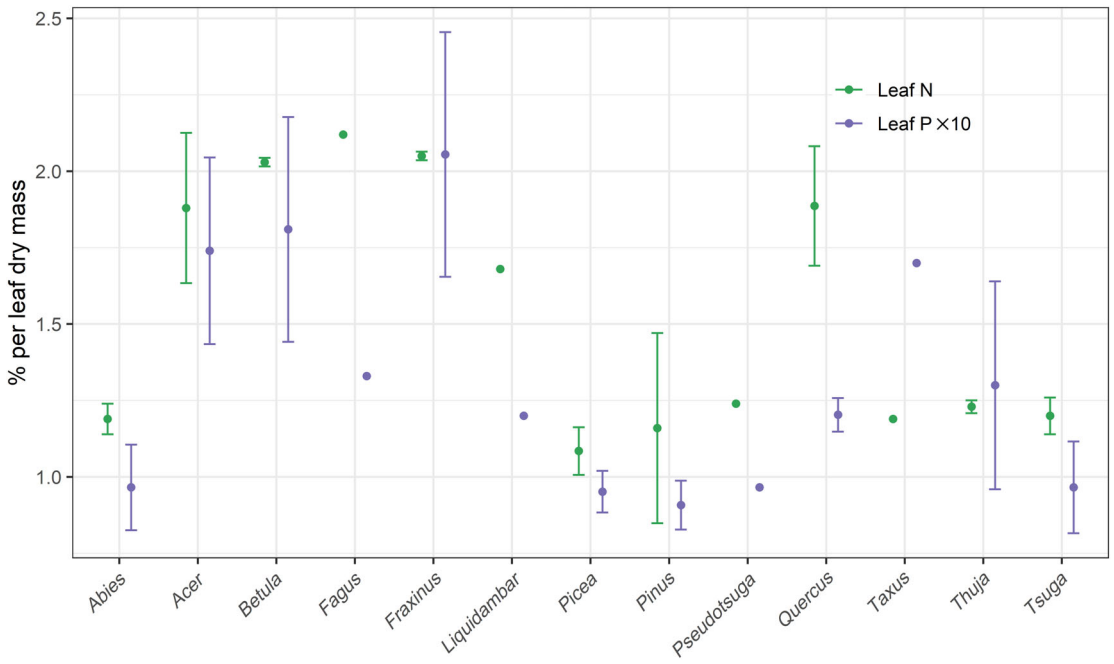

FIGURE 2 Mean and standard deviation of foliar nutrient concentrations (i.e., nitrogen and phosphorous) for the genera included in this study. Data came from the authors and were supplemented with the TRY Plant Trait Database (Kattge et al., 2020). Values of foliar phosphorous were multiplied by 10 so they could be plotted with foliar nitrogen.

resolving individual variation. Field measurements and laboratory analysis have been widely used to quantify *foliar* nutrient concentration (Perez-Harguindeguy et al., 2013). However, the large investments required for data collection and analysis have limited application. By contrast, airborne imaging spectroscopy (also known as hyperspectral remote sensing) now offers an alternative approach to consistently estimate *crown* nutrient concentrations regionally in a wide range of forest types such as tropical (Asner et al., 2015), temperate (Singh et al., 2015; Wang et al., 2020), and boreal forests (Ollinger et al., 2008). Hyperspectral data from the NEON Airborne Observation Platform (AOP) provides consistent and open-access products with continental coverage (Figure 3). In addition, recent models (Wang et al., 2020, 2022) have been developed with leaf spectral and laboratory assays from 1,103 individuals and 236 species across the NEON domains in the United States. The light detection and ranging (LiDAR) instrument on the AOP can be used for crown delineation (Dalponte & Coomes, 2016), enabling the derivation of foliar estimates for individual trees (Figure 4). Taken together, the combined LiDAR and hyperspectral imaging from NEON AOP offers unprecedented opportunities to derive foliar nutrients at the individual scale and to quantify their effects on fecundity for the same trees across broad biogeographic regions.

Understanding the effects of foliar nutrients within species requires estimates of seed production at the individual scale across landscapes and regions. Nutrient additions to individual trees (Brown et al., 1995; Rosecrance et al., 1998) show that applied nitrogen (Davis et al., 2004; Ran et al., 2008), phosphorous (Ran et al., 2008), potassium (Ran et al., 2008), and calcium (Halman et al., 2013) can increase yield (scale A). Insights from orchard practice add to the limited literature from natural settings (Han et al., 2008; Ichie & Nakagawa, 2013; Miyazaki et al., 2014; Sala et al., 2012). These controlled studies and monitoring

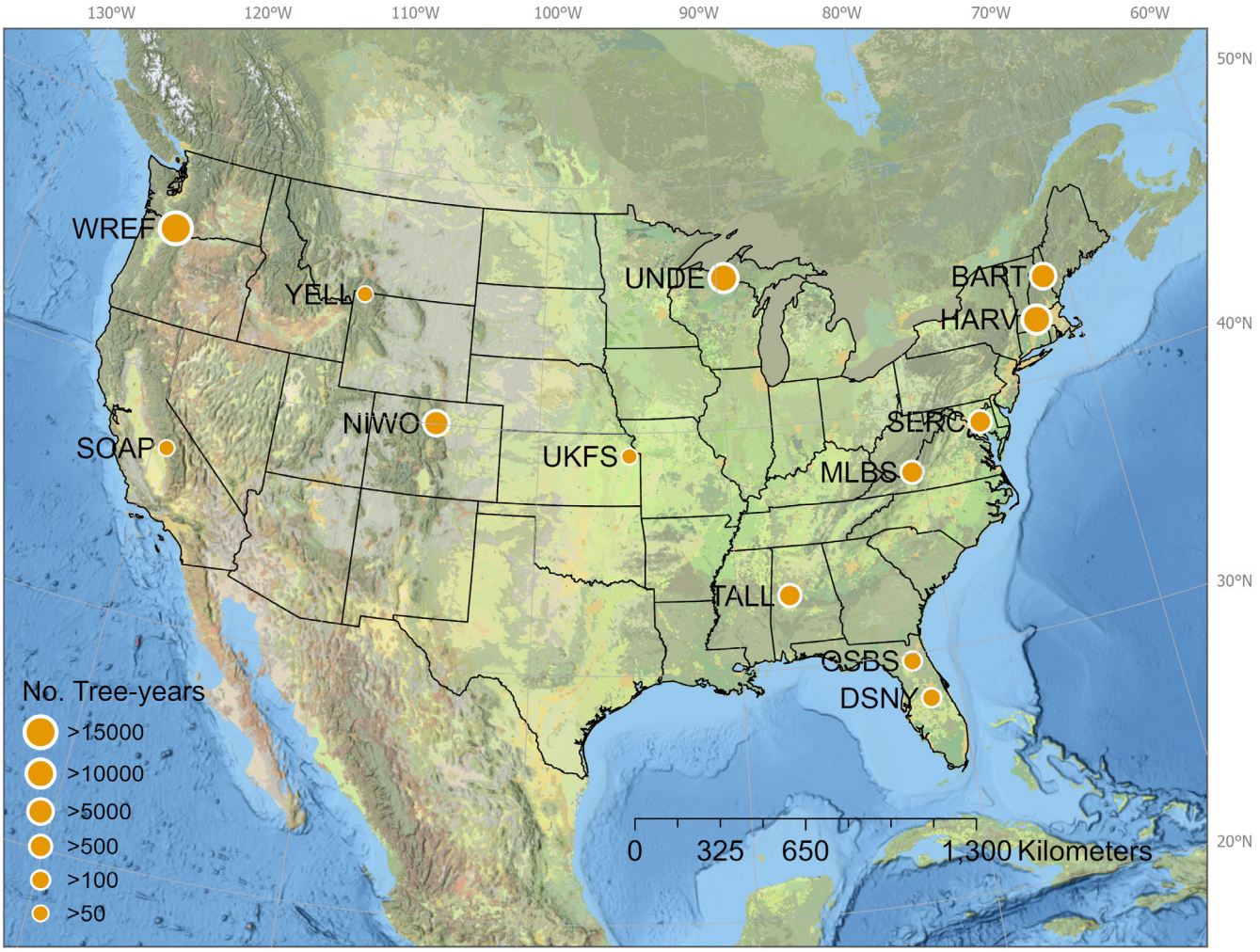

FIGURE 3 This study includes 13 sites from the National Ecological Observatory Network (NEON) that span the contiguous United States. Site descriptions can be found in Table 1 in the main text. Point size scales with the number of tree-year observations for reproduction estimation at each site. Sample size (i.e., plot, trees, and tree-years) can be found in Appendix S1: Table S1.

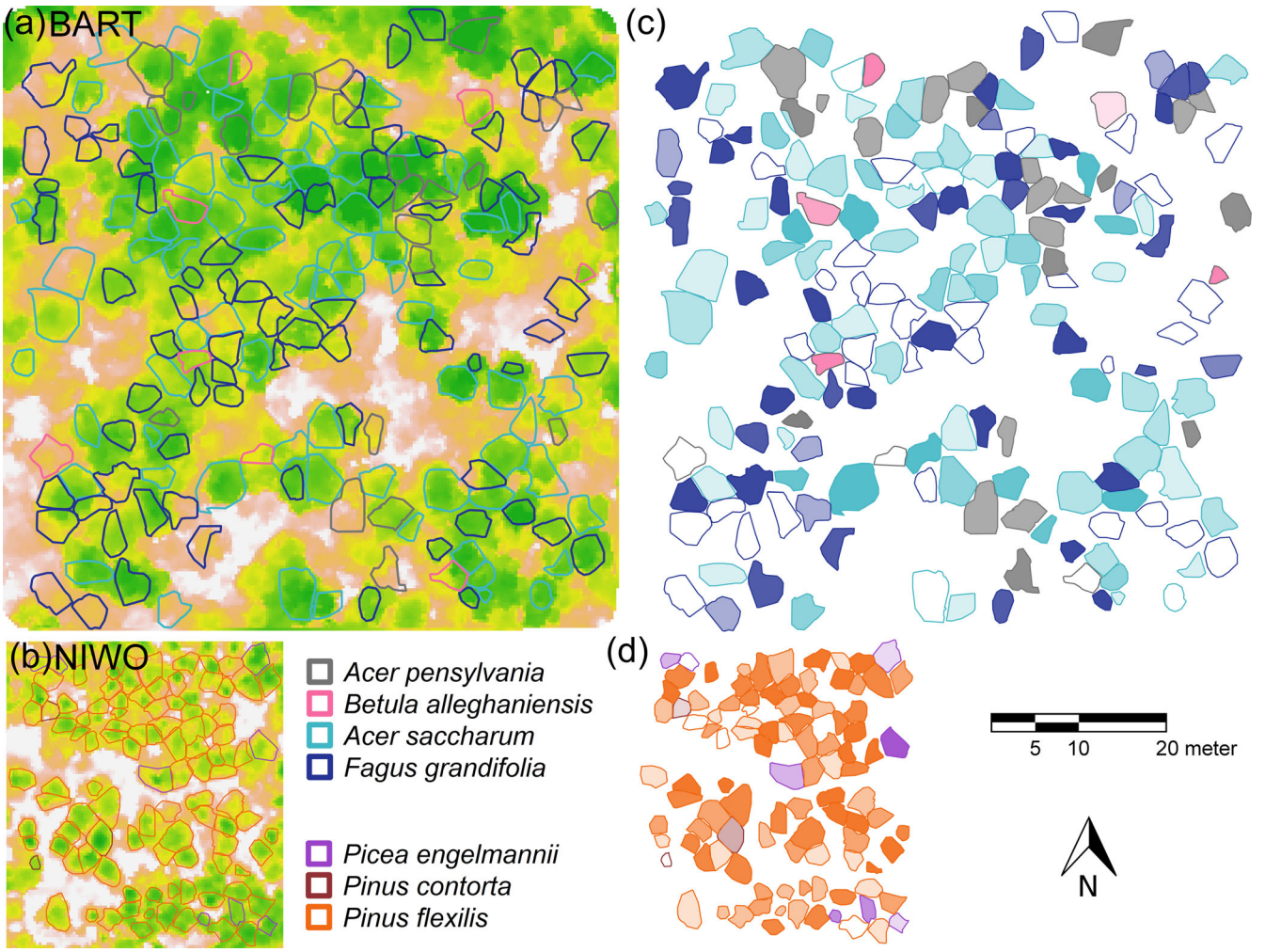

FIGURE 4 Crown delineation in a deciduous-dominant large plot at Bartlett Experimental Forest (BART, panel a) and a conifers-dominant small plot at Niwot Ridge (NIWO, panel b). The canopy height model is shown in the background, where green means a high value and brown indicates a low value. Mature individuals with fecundity estimates (see *Materials and methods*) are colored by their species. Fecundity at each tree crown is summarized in panels (c) and (d), where higher transparency indicates low fecundity and vice versa. More examples of crown delineation can be found in the Appendix S1: Figure S2.

of changes within a tree over time do not resolve the respective roles of direct effects on reproduction from the indirect effects that come from growth stimulation and, thus, increased size (LaDeau & Clark, 2001; Qiu, Aravena, et al., 2021). Moreover, the responses of individuals to changes in nutrient status (nutrient addition) might not be the same as the effects of natural fertility gradients on individuals subjected to one habitat throughout their lives. To evaluate the role of variation between individuals subjected to variation in fertility (scale B), we define the individual seed production (ISP) relative to tree basal area:

$$\mathrm{ISP}_{ijs} = \frac{\widehat{f}_{ijs} \times g_s}{\text{basal area}_i} \quad (1)$$

For tree i at location j of species s, ISP depends on mass per seed (g_s) and number of seeds ($\widehat{f}_{ijs}$) per basal area (Journe et al., 2022; Qiu et al., 2022). Our definition of ISP incorporates year-to-year variation in fecundity and its uncertainty (see *Materials and methods*); these ISP values are combined with foliar nutrient status to evaluate species differences and individuals within species.

We hypothesized that the association between individual nutrient status and seed production depends on species-specific allocation to reproduction (scale B). Horticultural research shows that fertilization, particularly with primary macronutrients N, P, and K (i.e., scale A), can stimulate reproduction (Marschner, 2011; Oosterhuis et al., 2014; Warner et al., 2004) or growth at the expense of reproduction, depending on the ratios (Faust, 1989; Neilsen & Neilsen, 2002; Rubio Ames et al., 2020; Weinbaum et al., 1992). Because the macronutrients Ca and Mg can be low in acidic soils (Aggangan et al., 1996; Han et al., 2019; Myers & Campbell, 1985) where many

conifers may dominate (Alfredsson et al., 1998; Iwashima et al., 2012), these nutrients could affect fecundity differently for these species groups.

While estimates of ISP can inform how individual reproduction is associated with nutrients, community seed production (CSP_j) at location j quantifies the biomass of seed produced per area of forest and provides the foundation to evaluate landscape-scale regeneration potential (scale D). CSP might exhibit limited sensitivity to nutrient availability because species turnover along fertility gradients could potentially compensate for within-species responses (Qiu et al., 2022). It is also possible that variation in CSP could be controlled by resource allocation trade-offs between growth and reproduction, similar to that of the ISP. Again, individual fertility status could diverge from spatially gridded products available in previous studies.

To determine the contribution of individual fertility to fecundity, we synthesized ISP and CSP with foliar N, P, K, Ca, and Mg concentrations from hyperspectral imagery across the NEON domain. A large sample size is required to estimate tree fecundity due to the low signal-to-noise ratio in seed production data, where tree-to-tree and year-to-year variation can vary by orders of magnitude (Clark et al., 2021; Qiu et al., 2023). The MASTIF network (Clark et al., 2019) provides an analytical framework that combines raw tree-year observations, individual tree size (Qiu, Aravena, et al., 2021) and local competition (Clark et al., 2004), temperature and moisture deficit (Journe et al., 2022), and habitat conditions. Generalized joint attribute modeling (GJAM) is used to quantify species responses, allowing for their dependence in response to nutrient availability; GJAM further accommodates the dominance of zeros in the data. Both MASTIF and GJAM are hierarchical Bayesian models and quantify the uncertainties in the data, model, and parameters.

MATERIALS AND METHODS

Our analysis involves three elements. We first quantified seed production by synthesizing individual tree-year observations and environmental covariates within a MASTIF framework (Clark et al., 2019, 2021), which accommodates dependence in seed production between trees and within trees over time. We then derived nutrients and their uncertainties for each individual tree crown using combined LiDAR and hyperspectral imagery. Finally, we estimated within-species coefficients of seed production to crown nutrients using a GJAM. We also quantified the effects of foliar nutrients on CSP using multiple linear regression. Our analysis included 13 NEON sites across the contiguous United States (Table 1) where both seed production and crown nutrients are available. There are a total of 11,331 mature trees and 56,544 tree-years (Figure 3; Appendix S1: Table S1).

Fecundity data and modeling

The fecundity data from the 13 NEON sites are part of the MASTIF network (Clark et al., 2019, 2021). MASTIF includes two types of raw data, seed traps (ST) and crop counts. ST data were the number of seeds from seed traps that were associated with individual trees from the

TABLE 1 National Ecological Observatory Network (NEON) sites used in this study, including their dominant vegetation types and the selected year of imagery NEON Airborne Observation Platform (AOP) used to estimate foliar traits. Locations are shown in Figure 3.

Site code	Site name	Dominant vegetation type	AOP year
BART	Bartlett Experimental Forest	Deciduous forest	2019
DSNY	Disney Wilderness Preserve	Evergreen forest, grassland, and wetland	2019
HARV	Harvard Forest	Deciduous and evergreen forest	2019
MLBS	Mountain Lake Biological Station	Deciduous forest	2017
NIWO	Niwot Ridge Mountain Research Station	Evergreen forest	2019
OSBS	Ordway-Swisher Biological Station	Evergreen forest	2019
SERC	Smithsonian Environmental Research Center	Deciduous forest	2017
SOAP	Soaproot Saddle	Evergreen and mixed forest	2017
TALL	Talladega National Forest	Deciduous and mixed forest	2017
UKFS	The University of Kansas Field Station	Deciduous forest and pasture	2018
UNDE	Notre Dame Environmental Research Center	Deciduous and mixed forest	2019
WREF	Wind River Experimental Forest	Evergreen forest	2018
YELL	Yellowstone National Park	Evergreen forest and grassland	2018

mapped stands at the 13 NEON sites. Seed-trap data provide the most precise estimates for highly fecund species with well-dispersed seeds. They provide estimates even in dense stands where crop counts are difficult. However, it is important to note that the estimates of fecundity rely on seed transport, which is not well estimated for species that produce large seeds, especially those that rely on secondary dispersal by animals whose seeds rarely occur in traps that are not directly under the tree crown. Further, seed dispersal into and out of a given plot can influence fecundity estimates (Muller-Landau et al., 2008). Crop counts data provide complementary advantages to ST. The trees that are hardest to estimate from ST (few, large seeds) are easiest to count directly on trees. Crop counts data mainly came from counts with binoculars, including the estimate of the fraction of the observed crop. Data compilation, modeling, and computation are open-access in the R package *MASTIF*, with more details provided by Clark et al. (2019, 2021).

We estimate seed production with a hierarchical Bayesian State-space model (Clark et al., 2019) that includes individual tree attributes with environmental conditions to estimate their effects on tree maturation and conditional fecundity. For individual tree i of species s at stand j in year t, the expected seed production equals the product of maturation probability and conditional fecundity,

$$E\left(f_{ijs,t}\right)=\widehat{f}_{ijs,t}=\rho_{ijs,t}\widehat{\psi}_{ijs,t} \tag{2}$$

Maturation probability $\rho_{ijs,t}$ determines whether an individual tree is in the mature state. It is a one-way process, where a tree is mature ($\rho_{ijs,t}=1$) if it has been observed to produce seed in the past (i.e., $\left[\rho_{ijr,t}=1|\rho_{ij,t-1}=1\right]=1$) and immature ($\rho_{ijs,t}=0$) if known to produce no seed subsequently (i.e., $\left[\rho_{ijr,t}=1|\rho_{ij,t+1}=0\right]=0$). The maturation probability $\rho_{ijs,t}$ is estimated using a probit hidden-Markov model,

$$\begin{aligned}&\rho_{ijs,t}\sim\text{Bernoulli}\\&\times\left(\rho_{ijs,t-1}+\left(1-\rho_{ijs,t-1}\right)\rho_{ijs,t+1}\Phi\left(\beta_0^{(\rho)}+\beta_1^{(\rho)}d_{ijs,t}\right)\right)\end{aligned} \tag{3}$$

where $\Phi(\cdot)$ is the standard cumulative normal distribution, $d_{ijs,t}$ is the diameter, $\beta_0^{(\rho)}$ and $\beta_1^{(\rho)}$ are the parameters for the intercept and diameter, respectively. Conditional fecundity is determined by a process model that is log-normal and depends on environmental covariates, random effects of individual and year, and error,

$$\log\left(\widehat{\psi}_{ijs,t}\right)=\mathbf{x}'_{ijs,t}\boldsymbol{\beta}^{(x)}+\beta_{ijs}^{(w)}+\gamma_{g[ij]s,t}+\epsilon_{ijs,t} \tag{4}$$

where $\mathbf{x}_{it}$ is a design matrix holding diameter, shade, and environmental conditions (see the next paragraph). The coefficients for fixed and random effects are $\boldsymbol{\beta}^{(x)}$ and $\beta_{ijs}^{(w)}$, respectively. Year effects are $\gamma_{g[ij]s,t}$, which are random across groups g (i.e., species-ecoRegion) and fixed for year t to accommodate interannual variations that are not fully absorbed by the climate in the covariates. Gaussian error is $\epsilon_{ijs,t}$.

Covariates for fecundity modeling are selected based on their capability to explain important variations in seed production. Covariates in Appendix S1: Table S2 includes individual attributes of each tree (diameter and shade class) and environmental conditions (i.e., climate and soil). The quadratic term for the diameter is included to accommodate fecundity response to tree size, especially at a large size (Qiu, Aravena, et al., 2021). Shading class (1–5 where 1 means open space and 5 means fully shaded) quantifies the self-competition and competition with neighbors on seed production (Clark et al., 2004). Spring temperature (T) and annual accumulative moisture deficit (M) are included as site norms and year-to-year anomalies to account for the variations between sites and within sites across years. Moisture deficit is evaluated as the differences between potential evapotranspiration (PET) and precipitation (P). Climate variables were extracted from two gridded products, including Terraclimate (Abatzoglou et al., 2018) and CHELSA (Karger et al., 2017), and calibrated to sites that have local weather data. We implemented variable selection based on the deviance information criterion (DIC). Furthermore, climate variables with a limited range of variations are not included in the model fitting.

Individual and community seed production

Evaluating the response of seed production to nutrient availability requires both seed size and seed numbers (Qiu et al., 2022). Because seed production varies with tree size (Clark et al., 2014; Qiu, Aravena, et al., 2021), tree-level seed production, that is, ISP, is defined relative to the tree basal area (Journe et al., 2022; Qiu et al., 2022). Calculation of ISP incorporates year-to-year estimates and their uncertainty for tree i of species s in stand j,

$$\text{ISP}_{ijs}=\frac{m_s}{b_{ij}}\times\frac{\sum_t w_{ijs,t}\widehat{f}_{ijs,t}}{\sum_t w_{ijs,t}} \tag{5}$$

where m_s is seed mass (in grams), b_{ij} is basal area (in square meters), and weight $w_{ijs,t}$ is the inverse of the coefficient of variation (CV). We used CV instead of the predictive variance because the mean estimate tends to scale with its variance such that CV emphasize high values of

$\widehat{f}_{ijs,t}$, which are less noisy and more important than low values. All quantification of ISP is time averages from annual estimates. Therefore, ISP has units of gram per square meter, with year^{-1} omitted from the dimensions.

The CSP (Journe et al., 2022; Qiu et al., 2022) can help understand the collective effects of nutrient availability on seed production at a stand level. We calculated CSP by extending seed production over all trees and species within a mapped stand,

$$\mathrm{CSP}_j = \frac{1}{A_j}\sum_{is}\mathrm{ISP}_{ijs} \quad (6)$$

where A_j is the plot area (in hectares) for each plot. The CSP thus quantifies stand production, similar to NPP that represents stand-level vegetative production.

Crown nutrients

We obtained the hyperspectral data as orthorectified surface directional reflectance products provided by the NEON AOP. The data products (product ID DP1.30006.001) were organized by flightlines. The AOP imaging spectrometer measures 426 bands between 380 and 2500 nm with a spectral resolution of 5 nm and a spatial resolution of 1 m (Kampe et al., 2010). Hyperspectral data were collected around local solar noon time during the peak growing season. NEON implemented a radiance calibration and atmospheric correction to obtain the orthorectified surface reflectance through the ATCOR-4 algorithm (Karpowicz & Kampe, 2015). Although AOP could provide multiple-year hyperspectral data for a subset of NEON sites, many of the flightlines were contaminated by clouds and their shadows. For each flightline, AOP flight crews evaluated the percentage of cloud cover (CC) at three levels, including green (CC <10%), yellow (10%< CC <50%), and red (CC >50%). We visually inspected all green hyperspectral flightlines between 2017 and 2019 and selected the best quality imagery for each NEON site (Table 1). Following Wang et al. (2020), we applied the open-access Python module HyTools (https://github.com/EnSpec/HyTools-sandbox/) (Chlus et al., 2022) to implement the topographic correction and the bidirectional reflectance distribution function (BRDF) correction (Appendix S1: Figure S2). We created the imagery mosaic from the corrected flight lines and took the mean values for overlapping regions at each NEON site. We removed atmospheric absorption bands that were noisy and kept spectral regions 418.59–1335.04 nm, 1460.23–1770.72 nm, and 1986.06–2396.71 nm. There are a total of 354 bands on average across the NEON sites.

We generated wall-to-wall foliar nutrient maps by applying the partial least squares regression (PLSR) coefficients provided by Wang et al. (2020) to the hyperspectral surface reflectance data. The coefficients were obtained through calibration and validation using a variety of NEON sites and were available at the Ecological Spectral Model Library (https://ecosml.org/package/github/EnSpec/NEON-Trait-Models). Following Wang et al. (2020), uncertainties were defined as the standard error from the 200 permutations of the PLSR model. Five nutrients, including nitrogen (N), phosphorous (P), potassium (K), magnesium (Mg), and calcium (Ca), were analyzed based on their important roles in plant reproduction (Fernández-Martínez et al., 2017; Ran et al., 2008) and their relatively high accuracies in the PLSR model (Wang et al., 2020). The goal of our study is to leverage the full capacity of the trained PLSR model by directly applying it to the same training dataset. This strategy, known as in-sample prediction, was chosen not with the intention of forecasting performance on unseen data, but rather to maximize the prediction accuracy of crown nutrients at the same sites they were sampled. For crown nutrients N, P, K, Mg, and Ca, the in-sample prediction coefficients of determination (i.e., R^2) were 0.92, 0.7, 0.72, 0.82, and 0.71, respectively. The normalized root mean square error (NRMSE), calculated as RMSE divided by the data range, was 6.75%, 12.8%, 13.24%, 9.74%, and 10.81% for N, P, K, Mg, and Ca, respectively.

For mapped and mature trees with ISP estimates, we delineated their crowns using LiDAR data (Figure 4). We obtained discrete return LiDAR point cloud data from the NEON AOP (product ID DP1.30003.001), which provides three-dimensional coordinates of multiple return points from vegetation and other surfaces. We generated canopy height models (CHM) using the pit-free algorithm in Khosravipour et al. (2014). This method effectively reduces the artifacts typically associated with ground and low-vegetation returns, offering a more accurate representation of canopy height across the forested landscape. We then detected individual treetops using the local maximum filter (LMF) in Popescu and Wynne (2004) on the CHM. The LMF's search window was adapted based on tree size, ensuring that larger trees with correspondingly larger crown diameters were accommodated with appropriately sized windows. Once individual tree tops were identified, we employed a crown segmentation algorithm from Dalponte and Coomes (2016) to delineate the crowns of mature trees for which seed production estimates were available. Smaller, immature trees and those growing in the understory (see previous section), which do not have fecundity estimates, were excluded from the crown delineation process to ensure our analysis focused on mature individuals with measurable seed production.

To accurately quantify crown nutrients, we calculated the weighted mean nutrient concentration for each pixel within a delineated tree crown. This method involves assigning weights to each pixel based on the inverse of the CV because the estimate of crown nutrients scales with its standard deviation. This approach ensures that pixels with lower variability (and thus higher reliability) contribute more significantly to the overall nutrient estimate. Sparsely vegetated or shadowed pixels were removed using two criteria: normalized difference vegetation index (NDVI) <0.6 or near-infrared (NIR) reflectance <0.06 (Wang et al., 2020).

Analyses

We used GJAM to quantify the within-species coefficients of ISP to multiple crown nutrients. GJAM allows us to jointly quantify multiple nutrient effects on all species due to its allowance for different data types and the dominance of zero values–many species are absent from most observations (Clark et al., 2017). On the latent scale, the observation $\mathbf{w}_j$ at plot j holds the ISP (the averaged value over conspecific individuals) for S species and is represented by a length S vector:

$$\mathbf{w}_j \tilde{} MVN\left(\mathbf{B}'\mathbf{x}_j,\ \boldsymbol{\Sigma}\right) \quad (7)$$

where $\mathbf{B}$ is the $Q \times S$ matrix of species coefficients, the length-Q vector $\mathbf{x}_j$ represents the covariates, including the five crown nutrients (N, P, K, Ca, and Mg). Matrix $\boldsymbol{\Sigma}$ measures the $S \times S$ residual covariance, which accounts for the potential relationship between species. As a Bayesian framework, GJAM focuses more on the estimation of parameters and their uncertainty, rather than on their statistical significance. The credible intervals for each species in Appendix S1: Figure S2 summarize the magnitude and direction of individual nutrient effects on ISP. Because all species were modeled jointly, we did not implement model selection for each individual species, for example, removing crown nutrient predictors that contain zero in their credible intervals.

Clusters of tree species that share similar responses to crown nutrients can help to define forest communities. We define communities based on within-species coefficient to crown nutrients and variations in the predictor:

$$\mathbf{E} = \mathbf{B}'\mathbf{V}\mathbf{B} \quad (8)$$

where $\mathbf{V}$ is the covariance of predictors in the design matrix. Related species could share similar or different within-species coefficients to crown nutrients (i.e., columns in $\mathbf{B}$). Those similarities and differences can be further amplified by large spatial variances in the predictors (the matrix $\mathbf{V}$), leading to positive values in $\mathbf{E}$ for similar groups, and negative values for different ones (Clark et al., 2017). Therefore, matrix $\mathbf{E}$ can identify forest communities that share similar responses to crown nutrients. We implemented hierarchical clustering on the 26 species included in the study using the R function "hclust" in the *stats* package. We identified five distinct communities and named them using two letters of genus and species for the two most abundant species in each community.

To map the five forest communities across the continent, we used the Forest Inventory Analysis (FIA) data from Qiu, Sharma, et al. (2021). To increase the signal-to-noise ratio, we aggregated the 196,765 FIA plots into approximately 13,000 one-hectare plots using a K-means algorithm (Qiu, Sharma, et al., 2021). After that, we identified the dominant species (the most abundant ones) from the 26 species at each aggregated plot. We then assigned the community label (from the five clusters of the $\mathbf{E}$ matrix) to each plot.

Finally, we used multiple linear regression (MLR) to examine the response of CSP to multiple foliar nutrients at the stand level. Following the same procedure of crown-level nutrients, we calculate the weighted mean values of the foliar nutrients as the plot-level predictor in the MLR. We include interactions between N, P, and K because their combinations are widely used in horticultural practices.

RESULTS

The association between ISP and the three primary macronutrients N, P, and K varies widely between species (scale B in Figure 1). ISP declines with foliar P in the majority (70%) of species (brown shading in Figure 5a); increases with foliar P are observed primarily in conifers. The relationships with N and K vary between species to a greater degree than P (Figure 5a). For the nutrient-demanding genus *Acer* (Figure 2), foliar K is associated with high seed production in *A. rubrum* but low seed production in *A. saccharum*, *A. pensylvanicum*, and *A. circinatum*. Foliar N is associated with high ISP for most species in *Acer* (except *A. pensylvanicum*). Both foliar N and K are associated with low ISP in the nutrient-demanding *Quercus* (Figure 2). For conifers with low nutrient requirements (Figure 2), the effects of crown N and K show a biogeographic divide. Within-species associations are negative in eastern species (e.g., *Pinus strobus* and *Tsuga canadensis*), but positive in western species (e.g., *Picea rubens*, *Tsuga heterophylla*, and *Pseudotsuga menziesii*).

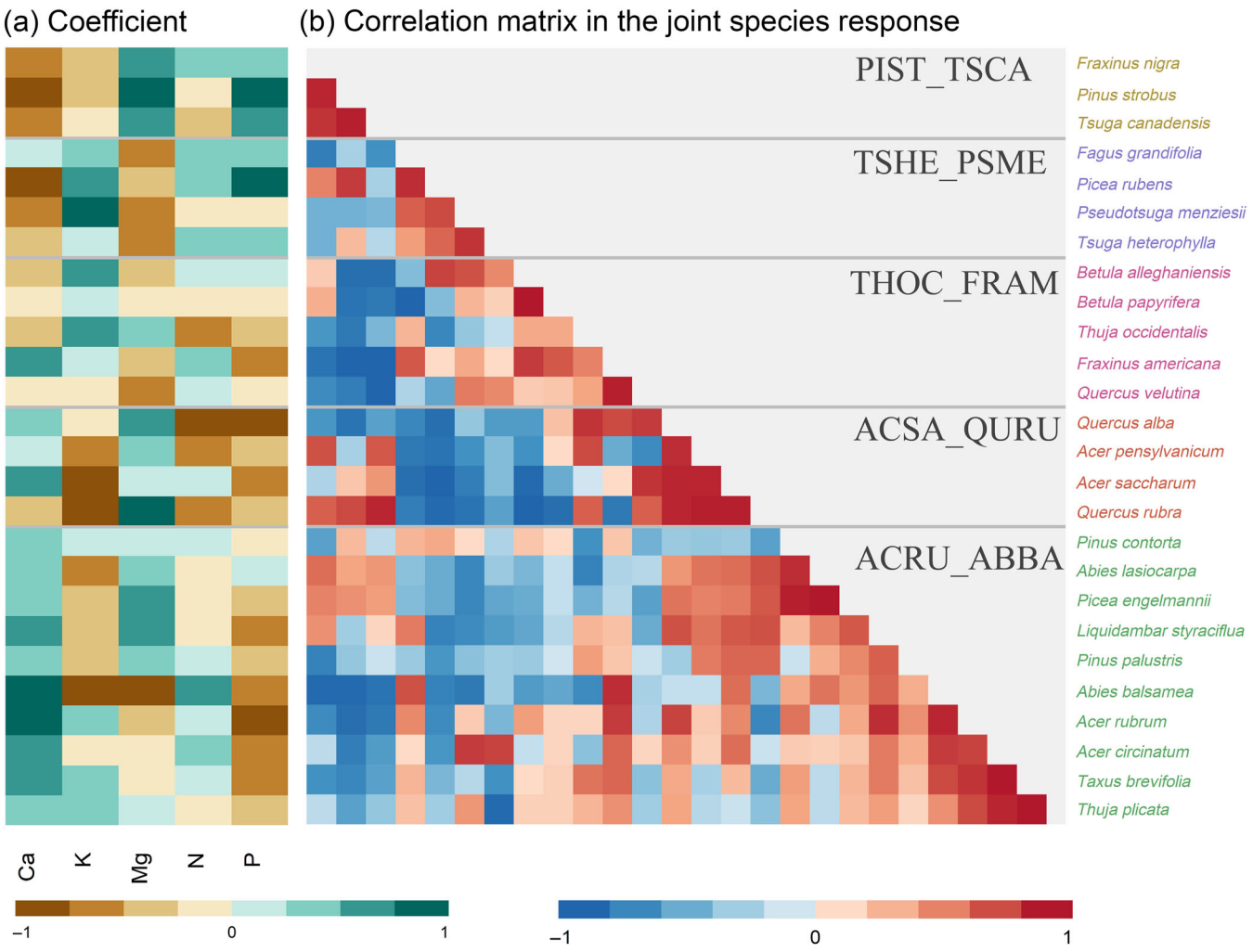

FIGURE 5 (a) Within-species coefficients of individual seed production (ISP, in grams per square meter tree basal area) to foliar nutrients (N, P, K, Ca, and Mg) using the posterior median from the fitted model. (b) Coefficient matrix (**E**) is used to group species with similar coefficients into five communities. Communities are separated by dashed lines. Communities are named using the first two letters of genus and species from the two most fecund species. For example, an eastern temperate community (*ACSA-QURU*) is negatively associated with N, P, K and positively associated with Ca and Mg. By contrast, western species in *TSHE-PSME* are positively associated with N, P, and K but negatively with Ca and Mg. Species labels are colored by their communities in Figure 6.

The two secondary macronutrients (i.e., Ca and Mg) show patterns that differ from primary macronutrients (i.e., N, P, K). Foliar Ca is associated with high seed production primarily in conifers, with exceptions being *Tsuga* and *Pinus strobus*. As for deciduous species, associations are positive for *Acer*, but negative in *Quercus*. Foliar Mg is associated with high reproduction in deciduous (e.g., *Quercus*) and coniferous (e.g., *Pinus*) species. It is worth noting that *Betula papyrifera* and *Pinus cortata* exhibited a limited response to all five macronutrients.

Similarities in the within-species coefficients of ISP to foliar nutrients (Figure 5a) define five communities in Figure 5b. ISP of species in northeastern montane forests *PIST-TSCA* share affinities for high foliar P and Mg and low foliar N, K, and Ca. In eastern temperate *ACSA-QURU* forests, low foliar N, P, and K and high foliar Ca and Mg are associated with high fecundity. By contrast, the eastern *THOC-FRAM* is associated with high foliar N and K and low foliar P, Ca, and Mg. The western *TSHE-PSME* contains species associated with high foliar N, P, and K but low foliar Ca and Mg. The *ACRU-ABBA* group is a heterogeneous collection of eastern and western species that associates with low foliar P and high foliar Ca. Overall, within-species differences cluster as clear assemblages (red blocks along the diagonal in Figure 5b) with distinct biogeographic patterns in Figure 6a. Species having fecundity associated with high foliar P (i.e., purple points of *TSHE-PSME*) mainly occur along the western coastlines.

Community seed production decreased by four orders of magnitude from >50,000 g/ha at the lowest foliar P to below 50 g/ha at the highest foliar P (Figure 7) (scale D

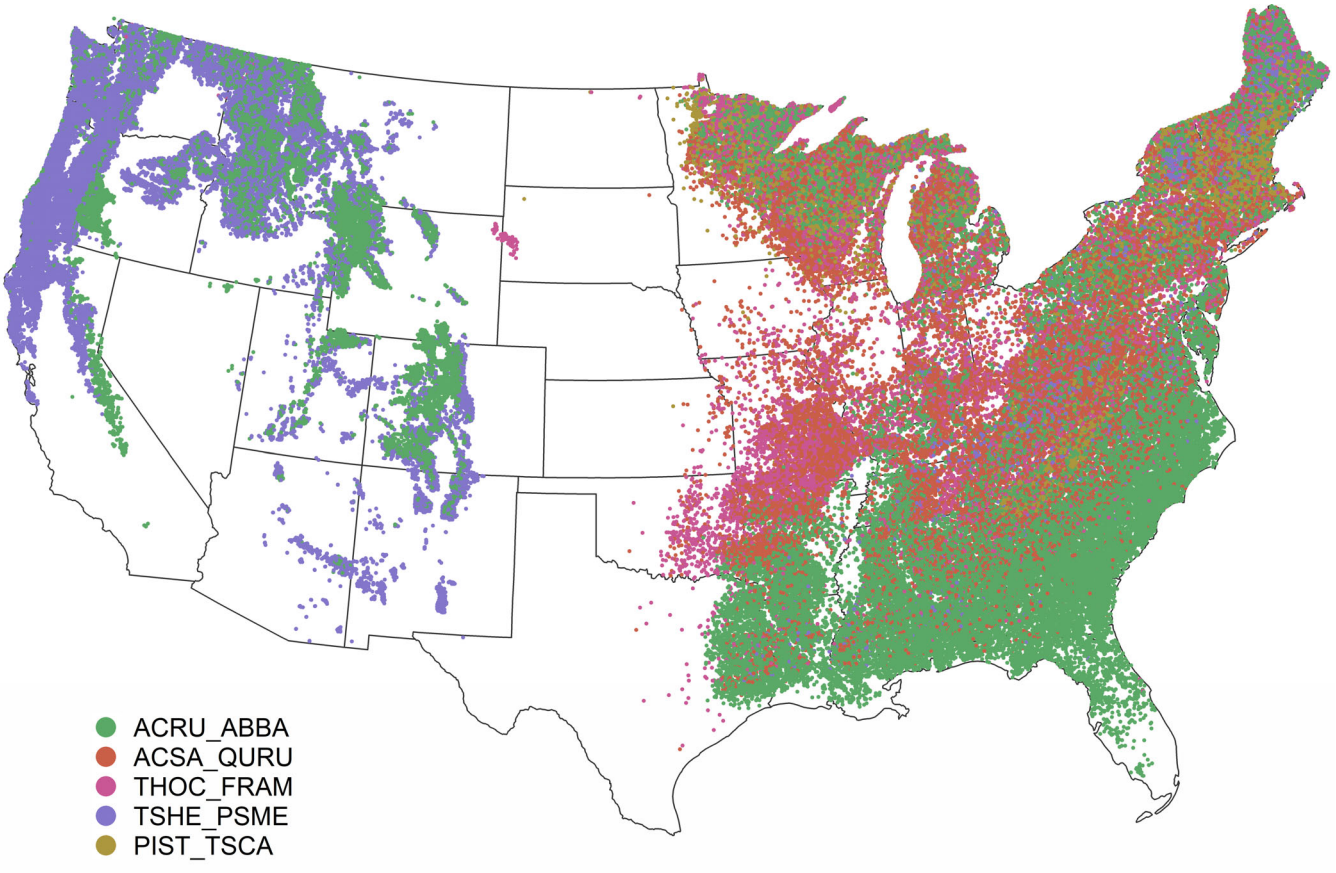

FIGURE 6 Map of species assemblages based on coefficients of seed production to crown nutrients. Each point is a plot from Forest Inventory Analysis (FIA). Community name and color follows Figure 5.

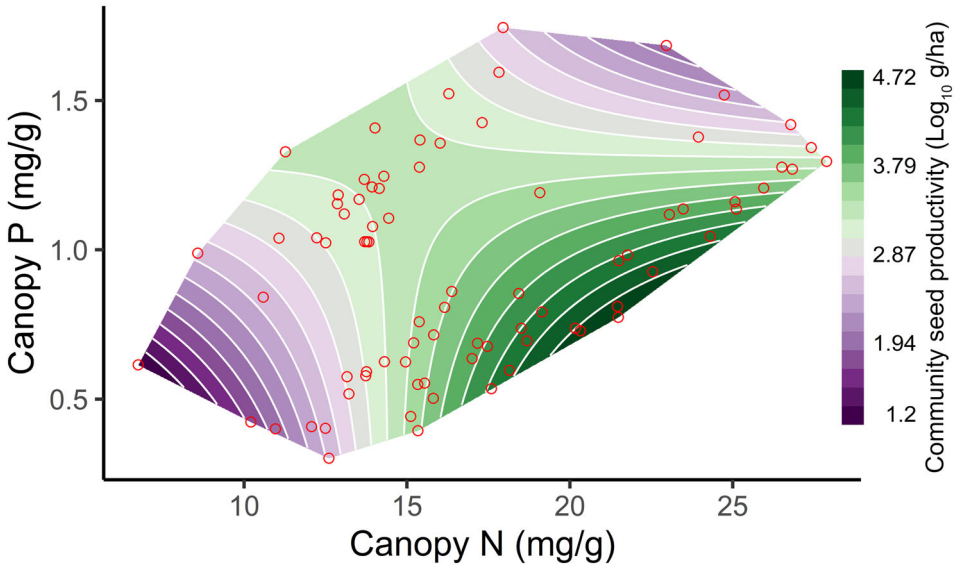

FIGURE 7 The effects of foliar N and P on community seed production (CSP; in grams per hectare) from the model in Appendix S1: Table S3 (i.e., positive main effects and negative interactions). The convex hull is constrained by the observations (red). Predictive standard error can be found in Appendix S1: Figure S4.

in Figure 1). The decline in CSP along the foliar P gradient is primarily driven by the negative within-species coefficients in ISP (Figure 5a). By contrast, high foliar N is associated with high CSP, especially at low foliar P levels (Figure 7b). Foliar K, Ca, and Mg show weak associations with CSP (Appendix S1: Table S3).

DISCUSSION

The pervasive association between high foliar P and low ISP emerges from the direct comparisons of tree fecundity and crown condition at the continental scale. This association holds at the individual scale B (variation within a species) (Figure 5) and across geographic space that varies in stand canopy P (scale D) (Figure 7). The hypothesized connections between seed production and nutrient storage in the literature (Fernández-Martínez et al., 2017; Han et al., 2008; Ichie & Nakagawa, 2013; Sala et al., 2012) rely on empirical evidence that is constrained, both geographically and taxonomically, due to limited individual-scale data. The recent finding that nutrient-demanding species, identified as those with high foliar P, tend to have low seed production (Qiu et al., 2022) (scale C) is consistent with this study that brings in individual nutrient status. Thus, intraspecific responses for most species (Figure 5a) (scale B) are consistent with interspecific differences in the fecundity-phosphorous relationship (Qiu et al., 2022) (scale C). The finding that high crown P is associated with low fecundity could result from growth stimulation at high P at the expense of reproduction (Elser et al., 2000; Weinbaum et al., 1992). However, the explanations for such trade-offs would operate differently at each of the four scales (Figure 1).

Our findings are not necessarily at odds with nutrient addition in horticultural practice, because they engage a different scale. Added N (Callahan et al., 2008; Davis et al., 2004; Ran et al., 2008) and K (Ran et al., 2008) can stimulate crop yield (scale A) or not (*Picea glauca* in Leeper et al. (2020), *Quercus suber* in Pérez-Ramos et al. (2014)). We found that the effects of N and K on ISP are associated with differing species' nutrient demands (Figure 5). In nutrient-demanding species, high seed production is associated with lower N and K in *Quercus*, and lower K in *Acer*. An increase in the availability of N and K could enhance a plant's growth and reduce seed production, due to the trade-off between allocating resources to biomass increase or to reproductive output (Qiu et al., 2022). By contrast, nutrient-conservative conifers exhibit a biogeographic divide, with positive relationships occurring mainly in the west, including *P. rubens*, *T. heterophylla*, and *P. menziesii* (Figure 5). This is consistent with previous findings that optimal levels of N and K, particularly for nutrient-conservative species, could stimulate reproduction (Ran et al., 2008).

Despite a tendency for conifers to occupy soils with low pH, high fecundity was associated with Ca in many species (e.g., all *Abies*, *Picea engelmannii*, *P. palustris, Taxus brevifolia, Thuja plicata*). The positive association in this study between crown Ca and fecundity within the deciduous species *Acer*, *Quercus*, and *Fagus* (Figure 5) complements previous findings of Ca stimulation in *Acer saccharum* (Halman et al., 2013; Long et al., 2011). Ca is a critical component of the cell wall, providing structural stability to plant cells (Thor, 2019). In the context of seed development, stronger cell walls can contribute to healthier seed coats, enhancing the viability of seed production. Compared with N, P, K, and Ca, the effects of crown Mg remain rarely studied. We found that high seed production is associated with high crown Mg in the eastern deciduous and coniferous species, including *Pinus*, *Quercus*, and *Acer* (except *A. rubrum*) (Figure 5). This positive relationship could be related to Mg's role in carbohydrate allocation from leaves to seeds (Geng et al., 2021).

Beyond introducing individual nutrient status, results reported here reflect an extension in sample size (56,544 tree-years for 26 species while previous studies include few species) and quantification of ISP (standardized by tree size). Perhaps still most important is the use of individual nutrient status rather than site values based on soil concentrations. For example, the rates of nutrient mineralization can diverge from soil concentrations, and rates of N mineralization are not available in most studies.

The fact that CSP (i.e., seed mass per forest floor area) decreases by approximately four orders of magnitude along the low-to-high foliar P gradient (Figure 7, scale D) is consistent with the negative within-species response to crown P for a given tree size (ISP) (Figure 5, scale B). By contrast, there is a positive relationship between CSP and foliar N (Figure 7), despite the fact that within-species response to crown N is mixed (46% negative and 54% positive) (Figure 5). It is worth noting that the positive relationship only occurs at low foliar P levels due to the positive main effects of N and the negative interaction between N and P (Figure 7; Appendix S1: Table S3). In addition, CSP does not respond to other nutrients (Appendix S1: Table S3). The large differences between the coefficients of individual-level and community-level seed production to N, K, Ca, and Mg could be caused by the neutralizing effects of divergent responses within species (Figure 5). Moreover, species turnover can result in CSP that is as high in low-nutrient as in high-nutrient communities (Qiu et al., 2022).

Tree seed production can be geographically coherent within species (Ascoli et al., 2017; LaMontagne et al., 2020), while still varying widely between species (Qiu et al., 2022) and even between individuals of the same species (Figure 5). The results here add insights to previous studies that focused on tree size (Clark et al., 2021; Qiu, Aravena, et al., 2021), climate (Clark et al., 2021; Journe et al., 2022), and soil fertility (Qiu et al., 2022), highlighting the importance of tracking ISP across the landscape.

Findings from this study could not have come from traditional measurements of crown nutrients that are time-consuming and expensive (Perez-Harguindeguy et al., 2013). Combined LiDAR and hyperspectral imagery allows the quantification of multiple crown nutrients at individual crowns (Figure 4), offering a direct connection to ISP.

The interannual variability in crown nutrient concentrations and its subsequent impact on seed production (scale A) represents an important future research direction. Our analyses primarily focused on spatial variations across trees (scale B, Figure 5) and communities (scale D, Figure 7). If multiyear crown nutrients were available, we might observe changes in nutrients following a seed production year (Han et al., 2008; Sala et al., 2012). However, our ability to test this hypothesis is constrained by the quality of available AOP hyperspectral data. Cloud cover and shadows, prevalent in many AOP flight lines, have limited the consistency and reliability of multiyear datasets. Future work that aims to mitigate the impact of data quality issues could provide valuable insights into the year-to-year variability in crown nutrients and their relationship with reproduction. Additionally, studies suggest that year-to-year seed production also responds to variables that could not be incorporated into this analysis, including disease and the historical context of forests (Pearse et al., 2021). The integration of these factors into our analysis was constrained by the availability and spatial distribution of data across the NEON sites.

The NEON AOP hyperspectral data, while being among the best available for ecological research, is not without its limitations. The effectiveness of the ATCOR atmospheric correction method depends heavily on the precision with which atmospheric conditions are modeled at the time of data acquisition. This dependency can sometimes lead to uncertainties in the data products (Richter & Schlapfer, 2011). Looking forward, advancements in sensor technology, particularly those with higher signal-to-noise ratios, alongside the evolution of space-borne imaging spectroscopy, promise significant enhancements in trait estimations. Space-borne sensors can provide broader coverage and more consistent data collection (Gholizadeh et al., 2022), but their relatively coarse spatial resolution poses a challenge for detecting fine-scale species composition variations that are essential for accurate trait analysis (Figure 4). This gap underscores the pressing need to either incorporate high-resolution data that can capture these critical details (Figure 4) or to develop new trait models based on the next generation of space-borne data (Cawse-Nicholson et al., 2021; Sousa & Small, 2023).

The structural complexity within canopies, including the arrangement of branches and the density of foliage, could influence the canopy's optical reflectivity and thus influence the estimation of foliar traits (Kamoske et al., 2021). The focus of AOP data collection on the canopy top is not a methodological constraint. For most of the species, we found seed production decreases from the exposed outer crown to the shaded interior (Qiu, Aravena, et al., 2021). Furthermore, it is crucial to recognize that factors such as within-tree variation in leaves and branches nutrients can also affect fecundity. These factors, although not the primary focus of our current analysis due to the data availability, represent important dimensions for future research.

Understanding forest regeneration requires the quantification of seed production. Fecundity is represented in the DGVMs as a constant fraction of NPP (Fisher et al., 2018; Hanbury-Brown et al., 2022). The fact that both individual-level and community-level seed production declines at high P (Figures 5 and 7), contrasts with the positive nutrient impacts on NPP (Alvarez-Clare et al., 2013; Menge et al., 2012) in models. The nutrient relationship here, at individual, species, and landscape scales has immediate application to forest regeneration in models that operate on multiple scales.

AUTHOR CONTRIBUTIONS

Tong Qiu and James S. Clark designed the study and performed the analyses. Tong Qiu, James S. Clark, and Jennifer J. Swenson co-wrote the paper. Kyle R. Kovach and Philip A. Townsend provided the hyperspectral data processing tools and revised the paper.

ACKNOWLEDGMENTS

For access to sites and logistical support, we thank the National Ecological Observatory Network (NEON). This project has been funded by the National Science Foundation DEB-1754443, the Belmont Forum (1854976), the National Aeronautics and Space Administration (NASA) Advanced Information Systems Technology (16-0052, 18-0063) and NASA Earth Science Applications: Ecological Conservation (80NSSC23K1534). It is also funded by the Programme d'Investissement d'Avenir under project FORBIC (18-MPGA-0004) (Make Our Planet Great Again). Philip A. Townsend and Kyle R. Kovach were supported by NSF Macrosystems Biology and NEON-Enabled Science grant DEB-1638720 and NSF Biology Integration Institute award DBI-2021898.

CONFLICT OF INTEREST STATEMENT

The authors declare no conflicts of interest.

DATA AVAILABILITY STATEMENT

Data (Qiu, 2024) supporting the findings are available in Dryad at https://doi.org/10.5061/dryad.4j0zpc8j7. Code (Qiu et al., 2024) is available in Zenodo at https://doi.org/

10.5281/zenodo.11246436. Seed production data (Clark et al., 2020) are available in the Duke Research Data Repository https://doi.org/10.7924/r4348ph5t. LiDAR and hyperspectral data are available in the National Ecological Observatory Network (NEON) data portal at https://data.neonscience.org/data-products/DP1.30003.001 (NEON, 2022a) and https://data.neonscience.org/data-products/DP1.30006.001 (NEON, 2022b), respectively.

ORCID

Tong Qiu https://orcid.org/0000-0003-4499-437X
Philip A. Townsend https://orcid.org/0000-0001-7003-8774

REFERENCES

Abatzoglou, J. T., S. Z. Dobrowski, S. A. Parks, and K. C. Hegewisch. 2018. "TerraClimate, a High-Resolution Global Dataset of Monthly Climate and Climatic Water Balance from 1958–2015." *Scientific Data* 5: 170191.

Aggangan, N. S., B. Dell, and N. Malajczuk. 1996. "Effects of Soil pH on the Ectomycorrhizal Response of *Eucalyptus urophylla* Seedlings." *New Phytologist* 134: 539–546.

Alfredsson, H., L. M. Condron, M. Clarholm, and M. R. Davis. 1998. "Changes in Soil Acidity and Organic Matter Following the Establishment of Conifers on Former Grassland in New Zealand." *Forest Ecology and Management* 112: 245–252.

Alvarez-Clare, S., M. C. Mack, and M. Brooks. 2013. "A Direct Test of Nitrogen and Phosphorus Limitation to Net Primary Productivity in a Lowland Tropical Wet Forest." *Ecology* 94: 1540–51.

Ascoli, D., G. Vacchiano, M. Turco, M. Conedera, I. Drobyshev, J. Maringer, R. Motta, and A. Hacket-Pain. 2017. "Inter-annual and Decadal Changes in Teleconnections Drive Continental-Scale Synchronization of Tree Reproduction." *Nature Communications* 8: 2205.

Asner, G. P., R. E. Martin, C. B. Anderson, and D. E. Knapp. 2015. "Quantifying Forest Canopy Traits: Imaging Spectroscopy Versus Field Survey." *Remote Sensing of Environment* 158: 15–27.

Bazzaz, F. A., D. D. Ackerly, and E. G. Reekie. 2000. "Reproductive Allocation in Plants." In *Seeds: the ecology of regeneration in plant communities*, 2nd ed., edited by M. Fenner, 1–37. Oxford: CAB International.

Berdanier, A. B., and J. S. Clark. 2016. "Divergent Reproductive Allocation Trade-Offs with Canopy Exposure across Tree Species in Temperate Forests." *Ecosphere* 7: 10.

Brown, P. H., S. A. Weinbaum, and G. A. Picchioni. 1995. "Alternate Bearing Influences Annual Nutrient Consumption and the Total Nutrient Content of Mature Pistachio Trees." *Trees* 9: 158–164.

Callahan, H. S., K. Del Fierro, A. E. Patterson, and H. Zafar. 2008. "Impacts of Elevated Nitrogen Inputs on Oak Reproductive and Seed Ecology." *Global Change Biology* 14: 285–293.

Cawse-Nicholson, K., P. A. Townsend, D. Schimel, A. M. Assiri, P. L. Blake, M. F. Buongiorno, P. Campbell, et al. 2021. "NASA's Surface Biology and Geology Designated Observable: A Perspective on Surface Imaging Algorithms." *Remote Sensing of Environment* 257: 112349.

Chlus, A., Z. Ye, T. Zheng, N. Queally, E. Greenberg, and P. A. Townsend. 2022. "EnSpec/hytools: 1.3.0." Zenodo. https://doi.org/10.5281/zenodo.5997756.

Clark, J. S., R. Andrus, M. Aubry-Kientz, Y. Bergeron, M. Bogdziewicz, D. C. Bragg, D. Brockway, et al. 2021. "Continent-Wide Tree Fecundity Driven by Indirect Climate Effects." *Nature Communications* 12: 1242.

Clark, J. S., R. Andrus, M. Aubry-Kientz, Y. Bergeron, M. Bogdziewicz, D. C. Bragg, D. Brockway, et al. 2020. "Data from: Continent-Wide Tree Fecundity Driven by Indirect Climate Effects." Duke Research Data Repository. https://doi.org/10.7924/r4348ph5t

Clark, J. S., D. M. Bell, M. C. Kwit, and K. Zhu. 2014. "Competition-Interaction Landscapes for the Joint Response of Forests to Climate Change." *Global Change Biology* 20: 1979–91.

Clark, J. S., S. LaDeau, and I. Ibanez. 2004. "Fecundity of Trees and the Colonization-Competition Hypothesis." *Ecological Monographs* 74: 415–442.

Clark, J. S., D. Nemergut, B. Seyednasrollah, P. J. Turner, and S. Zhang. 2017. "Generalized Joint Attribute Modeling for Biodiversity Analysis: Median-Zero, Multivariate, Multifarious Data." *Ecological Monographs* 87: 34–56.

Clark, J. S., C. L. Nuñez, and B. Tomasek. 2019. "Foodwebs Based on Unreliable Foundations: Spatiotemporal Masting Merged with Consumer Movement, Storage, and Diet." *Ecological Monographs* 89: e01381.

Curtis, P. G., C. M. Slay, N. L. Harris, A. Tyukavina, and M. C. Hansen. 2018. "Classifying Drivers of Global Forest Loss." *Science* 361: 1108–11.

Dalponte, M., and D. A. Coomes. 2016. "Tree-Centric Mapping of Forest Carbon Density from Airborne Laser Scanning and Hyperspectral Data." *Methods in Ecology and Evolution* 7: 1236–45.

Davis, M. R., R. B. Allen, and P. W. Clinton. 2004. "The Influence of N Addition on Nutrient Content, Leaf Carbon Isotope Ratio, and Productivity in a Nothofagus Forest during Stand Development." *Canadian Journal of Forest Research* 34: 2037–48.

Duane, A., M. Castellnou, and L. Brotons. 2021. "Towards a Comprehensive Look at Global Drivers of Novel Extreme Wildfire Events." *Climatic Change* 165: 43.

Elser, J., R. Sterner, E. Gorokhova, W. Fagan, T. Markow, J. Cotner, J. Harrison, S. Hobbie, G. Odell, and L. Weider. 2000. "Biological Stoichiometry from Genes to Ecosystems." *Ecology Letters* 3: 540–550.

Faust, M. 1989. *Physiology of Temperate Zone Fruit Trees*. New York, NY: John Wiley and Sons, Inc.

Fernández-Martínez, M., S. Vicca, I. A. Janssens, J. M. Espelta, and J. Peñuelas. 2017. "The Role of Nutrients, Productivity and Climate in Determining Tree Fruit Production in European Forests." *New Phytologist* 213: 669–679.

Fisher, R. A., C. D. Koven, W. R. L. Anderegg, B. O. Christoffersen, M. C. Dietze, C. E. Farrior, J. A. Holm, et al. 2018. "Vegetation Demographics in Earth System Models: A Review of Progress and Priorities." *Global Change Biology* 24: 35–54.

Geng, G., I. Cakmak, T. Ren, Z. Lu, and J. Lu. 2021. "Effect of Magnesium Fertilization on Seed Yield, Seed Quality, Carbon

Assimilation and Nutrient Uptake of Rapeseed Plants." *Field Crops Research* 264: 108082.

Gholizadeh, H., A. P. Dixon, K. H. Pan, N. A. McMillan, R. G. Hamilton, S. D. Fuhlendorf, J. Cavender-Bares, and J. A. Gamon. 2022. "Using Airborne and DESIS Imaging Spectroscopy to Map Plant Diversity across the Largest Contiguous Tract of Tallgrass Prairie on Earth." *Remote Sensing of Environment* 281: 113254.

Halman, J. M., P. G. Schaberg, G. J. Hawley, L. H. Pardo, and T. J. Fahey. 2013. "Calcium and Aluminum Impacts on Sugar Maple Physiology in a Northern Hardwood Forest." *Tree Physiology* 33: 1242–51.

Han, Q., D. Kabeya, A. Iio, and Y. Kakubari. 2008. "Masting in Fagus Crenata and its Influence on the Nitrogen Content and Dry Mass of Winter Buds." *Tree Physiology* 28: 1269–76.

Han, T., A. Cai, K. Liu, J. Huang, B. Wang, D. Li, M. Qaswar, G. Feng, and H. Zhang. 2019. "The Links between Potassium Availability and Soil Exchangeable Calcium, Magnesium, and Aluminum Are Mediated by Lime in Acidic Soil." *Journal of Soils and Sediments* 19: 1382–92.

Hanbury-Brown, A. R., R. E. Ward, and L. M. Kueppers. 2022. "Forest Regeneration within Earth System Models: Current Process Representations and Ways Forward." *New Phytologist* 235: 20–40.

Ichie, T., and M. Nakagawa. 2013. "Dynamics of Mineral Nutrient Storage for Mast Reproduction in the Tropical Emergent Tree Dryobalanops Aromatica." *Ecological Research* 28: 151–58.

Iwashima, N., T. Masunaga, R. Fujimaki, A. Toyota, I. Tayasu, T. Hiura, and N. Kaneko. 2012. "Effect of Vegetation Switch on Soil Chemical Properties." *Soil Science and Plant Nutrition* 58: 783–792.

Journe, V., R. Andrus, M.-C. Aravena, D. Ascoli, R. Berretti, D. Berveiller, M. Bogdziewicz, et al. 2022. "Globally, Tree Fecundity Exceeds Productivity Gradients." *Ecology Letters* 25: 1471–82.

Kamoske, A. G., K. M. Dahlin, S. P. Serbin, and S. C. Stark. 2021. "Leaf Traits and Canopy Structure Together Explain Canopy Functional Diversity: An Airborne Remote Sensing Approach." *Ecological Applications* 31: e02230.

Kampe, T., B. Johnson, M. Kuester, and M. Keller. 2010. "NEON: The First Continental-Scale Ecological Observatory with Airborne Remote Sensing of Vegetation Canopy Biochemistry and Structure." *Journal of Applied Remote Sensing* 4: 043510.

Karger, D. N., O. Conrad, J. Böhner, T. Kawohl, H. Kreft, R. W. Soria-Auza, N. E. Zimmermann, H. P. Linder, and M. Kessler. 2017. "Climatologies at High Resolution for the Earth's Land Surface Areas." *Scientific Data* 4: 170122.

Karpowicz, B., and T. Kampe. 2015. "NEON Imaging Spectrometer Radiance to Reflectance Algorithm Theoretical Basis Document." NEON Document. NEON.DOC.001288

Kattge, J., G. Bönisch, S. Díaz, S. Lavorel, I. C. Prentice, P. Leadley, S. Tautenhahn, et al. 2020. "TRY Plant Trait Database – Enhanced Coverage and Open Access." *Global Change Biology* 26: 119–188.

Khosravipour, A., A. K. Skidmore, M. Isenburg, T. Wang, and Y. A. Hussin. 2014. "Generating Pit-Free Canopy Height Models from Airborne Lidar." *Photogrammetric Engineering & Remote Sensing* 80: 863–872.

LaDeau, S. L., and J. S. Clark. 2001. "Rising CO_2 Levels and the Fecundity of Forest Trees." *Science* 292: 95–98.

LaMontagne, J. M., I. S. Pearse, D. F. Greene, and W. D. Koenig. 2020. "Mast Seeding Patterns Are Asynchronous at a Continental Scale." *Nature Plants* 6: 460–65.

Leeper, A. C., B. A. Lawrence, and J. M. LaMontagne. 2020. "Plant-Available Soil Nutrients Have a Limited Influence on Cone Production Patterns of Individual White Spruce Trees." *Oecologia* 194: 101–111.

Long, R. P., S. B. Horsley, and T. J. Hall. 2011. "Long-Term Impact of Liming on Growth and Vigor of Northern Hardwoods." *Canadian Journal of Forest Research* 41: 1295–1307.

Marschner, H. 2011. *Marschner's Mineral Nutrition of Higher Plants*. Cambridge MA: Academic Press.

McDowell, N. G., C. D. Allen, K. Anderson-Teixeira, B. H. Aukema, B. Bond-Lamberty, L. Chini, J. S. Clark, et al. 2020. "Pervasive Shifts in Forest Dynamics in a Changing World." *Science* 368: eaaz9463.

Menge, D. N., L. O. Hedin, and S. W. Pacala. 2012. Nitrogen and Phosphorus Limitation over Long-Term Ecosystem Development in Terrestrial Ecosystems. *PLoS One 7*. https://doi.org/10.1371/journal.pone.0042045

Miyazaki, Y., Y. Maruyama, Y. Chiba, M. J. Kobayashi, B. Joseph, K. K. Shimizu, K. Mochida, T. Hiura, H. Kon, and A. Satake. 2014. "Nitrogen as a Key Regulator of Flowering in Fagus Crenata: Understanding the Physiological Mechanism of Masting by Gene Expression Analysis." *Ecology Letters* 17: 1299–1309.

Muller-Landau, H. C., S. J. Wright, O. Calderón, R. Condit, and S. P. Hubbell. 2008. "Interspecific Variation in Primary Seed Dispersal in a Tropical Forest." *Journal of Ecology* 96: 653–667.

Myers, D. F., and R. Campbell. 1985. "Lime and the Control of Clubroot of Crucifers: Effects of pH, Calcium, Magnesium, and Their Interactions." *Phytopathology* 75: 670–73.

Neilsen, D., and G. Neilsen. 2002. "Efficient Use of Nitrogen and Water in High-Density Apple Orchards." *HortTechnology* 12: 19–25.

NEON. 2022a. "Discrete Return LiDAR Point Cloud (DP1.30003.001)." National Ecological Observatory Network. [Dataset accessed May 1, 2022.] https://data.neonscience.org/data-products/DP1.30003.001.

NEON. 2022b. "Spectrometer Orthorectified Surface Directional Reflectance - Flightline (DP1.30006.001)." National Ecological Observatory Network. [Dataset accessed May 1, 2022.] https://data.neonscience.org/data-products/DP1.30006.001.

Ollinger, S. V., A. D. Richardson, M. E. Martin, D. Y. Hollinger, S. E. Frolking, P. B. Reich, L. C. Plourde, et al. 2008. "Canopy Nitrogen, Carbon Assimilation, and Albedo in Temperate and Boreal Forests: Functional Relations and Potential Climate Feedbacks." *Proceedings of the National Academy of Sciences* 105: 19336–41.

Oosterhuis, D. M., D. A. Loka, E. M. Kawakami, and W. T. Pettigrew. 2014. "The Physiology of Potassium in Crop Production." *Advances in Agronomy* 126: 203–233.

Pearse, I. S., A. P. Wion, A. D. Gonzalez, and M. B. Pesendorfer. 2021. "Understanding Mast Seeding for Conservation and Land Management." *Philosophical Transactions of the Royal Society B* 376: 20200383.

Perez-Harguindeguy, N., S. Diaz, E. Garnier, S. Lavorel, H. Poorter, P. Jaureguiberry, M. Bret-Harte, W. Cornwell, J. Craine, and D. Gurvich. 2013. "New Handbook for Standardised Measurement of Plant Functional Traits Worldwide." *Australian Journal of Botany* 61: 167–234.

Pérez-Ramos, I. M., C. Aponte, L. V. García, C. M. Padilla-Díaz, and T. Marañón. 2014. "Why Is Seed Production So Variable among Individuals? A Ten-Year Study with Oaks Reveals the Importance of Soil Environment." *PLoS One* 9: e115371.

Popescu, S. C., and R. H. Wynne. 2004. "Seeing the Trees in the Forest." *Photogrammetric Engineering & Remote Sensing* 70: 589–604.

Qiu, T. 2024. "Remotely Sensed Crown Nutrient Concentrations Modulate Forest Reproduction across the Contiguous United States." Dryad, Dataset. https://doi.org/10.5061/dryad.4j0zpc8j7.

Qiu, T., R. Andrus, M.-C. Aravena, D. Ascoli, Y. Bergeron, R. Berretti, D. Berveiller, et al. 2022. "Limits to Reproduction and Seed Size-Number Trade-Offs that Shape Forest Dominance and Future Recovery." *Nature Communications* 13: 2381.

Qiu, T., M.-C. Aravena, R. Andrus, D. Ascoli, Y. Bergeron, R. Berretti, M. Bogdziewicz, et al. 2021. "Is there Tree Senescence? The Fecundity Evidence." *Proceedings of the National Academy of Sciences* 118: e2106130118.

Qiu, T., M.-C. Aravena, D. Ascoli, Y. Bergeron, M. Bogdziewicz, T. Boivin, R. Bonal, et al. 2023. "Masting Is Uncommon in Trees that Depend on Mutualist Dispersers in the Context of Global Climate and Fertility Gradients." *Nature Plants* 9: 1044–56.

Qiu, T., S. Sharma, C. W. Woodall, and J. S. Clark. 2021. "Niche Shifts from Trees to Fecundity to Recruitment that Determine Species Response to Climate Change." *Frontiers in Ecology and Evolution* 9: 719141.

Qiu, T., J. S. Clark, K. R. Kovach, P. A. Townsend, and J. J. Swenson. 2024. "Remotely Sensed Crown Nutrient Concentrations Modulate Forest Reproduction across the Contiguous United States." Zenodo. https://doi.org/10.5281/zenodo.11246436.

Ran, E., D. Arnon, B.-G. Alon, S. Amnon, and Y. Uri. 2008. "Flowering and Fruit Set of Olive Trees in Response to Nitrogen, Phosphorus, and Potassium." *Journal of the American Society for Horticultural Science* 133: 639–647.

Richter, R., and D. Schlapfer. 2011. "Atmospheric/Topographic Correction for Airborne Imagery." ATCOR-4 User Guide. 565–602.

Rosecrance, R. C., S. A. Weinbaum, and P. H. Brown. 1998. "Alternate Bearing Affects Nitrogen, Phosphorus, Potassium and Starch Storage Pools in Mature Pistachio Trees." *Annals of Botany* 82: 463–470.

Rubio Ames, Z., J. K. Brecht, and M. A. Olmstead. 2020. "Nitrogen Fertilization Rates in a Subtropical Peach Orchard: Effects on Tree Vigor and Fruit Quality." *Journal of the Science of Food and Agriculture* 100: 527–539.

Sala, A., K. Hopping, E. J. B. McIntire, S. Delzon, and E. E. Crone. 2012. "Masting in Whitebark Pine (*Pinus albicaulis*) Depletes Stored Nutrients." *New Phytologist* 196: 189–199.

Singh, A., S. P. Serbin, B. E. McNeil, C. C. Kingdon, and P. A. Townsend. 2015. "Imaging Spectroscopy Algorithms for Mapping Canopy Foliar Chemical and Morphological Traits and their Uncertainties." *Ecological Applications* 25: 2180–97.

Sousa, D., and C. Small. 2023. "Topological Generality and Spectral Dimensionality in the Earth Mineral Dust Source Investigation (EMIT) Using Joint Characterization and the Spectral Mixture Residual." *Remote Sensing* 15: 2295.

Thor, K. 2019. "Calcium—Nutrient and Messenger." *Frontiers in Plant Science* 10: 440.

Wang, Z., A. Chlus, R. Geygan, Z. Ye, T. Zheng, A. Singh, J. J. Couture, J. Cavender-Bares, E. L. Kruger, and P. A. Townsend. 2020. "Foliar Functional Traits from Imaging Spectroscopy across Biomes in Eastern North America." *New Phytologist* 228: 494–511.

Wang, Z., P. A. Townsend, and E. L. Kruger. 2022. "Leaf Spectroscopy Reveals Divergent Inter-and Intra-Species Foliar Trait Covariation and Trait-Environment Relationships across NEON Domains." *New Phytologist* 235: 923–938.

Warner, J., T. Zhang, and X. Hao. 2004. "Effects of Nitrogen Fertilization on Fruit Yield and Quality of Processing Tomatoes." *Canadian Journal of Plant Science* 84: 865–871.

Weinbaum, S. A., R. S. Johnson, and T. M. DeJong. 1992. "Causes and Consequences of Overfertilization in Orchards." *HortTechnology* 2: 112b–21.

SUPPORTING INFORMATION

Additional supporting information can be found online in the Supporting Information section at the end of this article.

How to cite this article: Qiu, Tong, James S. Clark, Kyle R. Kovach, Philip A. Townsend, and Jennifer J. Swenson. 2024. "Remotely Sensed Crown Nutrient Concentrations Modulate Forest Reproduction across the Contiguous United States." *Ecology* 105(8): e4366. https://doi.org/10.1002/ecy.4366